Three-dimensional remote aggregation and steering of magnetotactic bacteria microrobots for drug delivery applications

Dominic de Lanauze, Ouajdi Felfoul, Jean-Philippe Turcot, Mahmood Mohammadi and Sylvain Martel

Abstract

Magnetotactic bacteria (MTB) can be viewed as self-propelled natural microrobots. These bacterial microrobots can be remotely controlled using magnetic fields due to their internal chain of iron-oxide nanoparticles acting like a compass needle. This internal chain enables them to adopt a magnetotactic behavior that can be exploited to perform a variety of microscale tasks from microassembly and micro-manufacturing to the delivery through microvascular networks of therapeutic agents to tumors. To effectively support these applications, three-dimensional (3D) aggregations of MTB become essential in order to manipulate and guide the bacteria effectively in the human microvasculature to deliver a predefined dose of therapeutics. To achieve such aggregations in a 3D volume, time-varying magnetic field sequences were developed enabling us to simulate in time the existence of a magnetic monopole. This article presents and compares three different time-varying magnetic field sequences generated by three orthogonal pairs of electromagnets able to generate such 3D aggregations of MTB.

Keywords

Magnetotactic bacteria, magnetotaxis, medical robotics, magnetic fields

1. Introduction

The miniaturization of robotic systems to the microscale has encountered serious setbacks. Technological limitations have prevented scientists and engineers from developing self-powered actuated microscale robots (Trimmer and Jebens, 1989; Dario et al., 1992; Abbott et al., 2007; Sharma and Mittal, 2008). Propulsion and steering are two of the main concerns when developing mobile microrobots. Different approaches using magnetic fields as an actuator have been proposed for interventions in the vascular network. Magnetic propulsion using the magnetic force exerted on a magnetic particle such as demonstrated in vivo in Martel et al. (2007) has encountered limitations since inducing a translational force on small particles to transit in capillary vessels requires a large amount of magnetic energy.

An alternative magnetic propulsion method uses magnetically controlled artificial nano-structured propellers (Ghosh and Fischer, 2009), helically symmetric flexible polymer structures (Piotr et al., 2009), and micrometer-scale artificial bacterial flagella (ABF) (Zhang et al., 2009; Tottori et al., 2012). ABF for instance are helical propellers being actuated using an induced magnetic torque generated by an external rotating magnetic field. Until now, flagella propulsion systems are still considered to be the best propulsion method in a low Reynolds number hydrodynamic regime. Since this type of device uses the magnetic torque as its propulsion and steering system, it requires less energy since the magnetic torque requires a less intense magnetic field compared to a pulling force.

Rather than focusing on the development of completely artificial microrobots, magnetotactic bacteria (MTB) (Blakemore, 1975; Faivre and Schüler, 2008), described in detail below, are considered to be natural microrobots. These natural microrobots have the distinct advantage of possessing molecular motors. Having its own natural autonomous propulsion system adapted to a low Reynolds hydrodynamic regime, each bacterium only requires a weak magnetic field for steering purposes. Besides the lower magnetic energy required compared to artificial structures

NanoRobotics Laboratory, Department of Computer and Software Engineering, Institute of Biomedical Engineering, École Polytechnique de Montréal (EPM), Campus of the Université de Montréal, Canada

Corresponding author:
Sylvain Martel, NanoRobotics Laboratory, Department of Computer and Software Engineering, Institute of Biomedical Engineering, École Polytechnique de Montréal (EPM), Campus of the Université de Montréal, P.O. Box 6079, Station Centre-ville, Montréal (Québec), H3C 3A7, Canada.
Email: sylvain.martel@polymtl.ca

due to their self-propelled characteristics, such MTB configurations allow their aggregation in a three-dimensional (3D) volume.

These microrobots are able to perform many tasks envisioned for futuristic artificial microrobots including but not limited to the micromanipulation (Sariola et al., 2008) or transport of micrometer-scale objects (Martel et al., 2006), coordinated microassembly of larger micro-objects (Martel and Mohammadi, 2010), magnetic separation of material in liquid environments (Bahaj et al., 1996), magnetic resonance imaging contrast agents (Benoit et al., 2009; Felfoul et al., 2010), and targeted drug delivery to tumors (Martel et al., 2009). While directional control of MTB is sufficient in certain applications, the ability to create, maintain, and control MTB aggregates is critical in many others.

For instance, in Martel et al.'s study (2010), a small computer-controlled electromagnet was positioned directly underneath a microscopically observed sample. This allowed our research group to aggregate MTB and select the size of the aggregations to increase the displacement force from individual MTB to a level suitable to move relatively large micro-objects. As described in Martel et al. (2009), when considering MTB as potential drug carriers, being able to aggregate a large number of drug-loaded MTB is critical for two reasons: to potentially achieve higher targeting efficacy and to deliver an adequate dose of therapeutics to a tumor. Therefore, our main concern in this article is to describe an efficient method to remotely aggregate MTB in 3D to take advantage of their inherent magnetotaxis (Lins de Barros et al., 1990).

MTB are microorganisms that synthesize membrane-bounded magnetic nanocrystals. These nanocrystals, known as magnetosomes (Frankel and Bazylinski, 1994; Faivre and Schüler, 2008), align in the cell in a chain-like fashion and enable the bacteria to respond to the presence of magnetic fields. This behavior occurs when the bacterium reacts to the magnetic torque exerted on it when the surrounding magnetic field and the magnetic moment of the chain are not parallel. Such behavior can be compared to the way a compass needle orients itself in parallel to the surrounding magnetic field. This property allows the MTB to orient themselves in their natural environment by making use of the Earth's magnetic field to propel themselves using their flagella towards their preferred chemical environment, usually a low oxygen concentration region (Spring and Bazylinski, 2006; Frankel et al., 2007). We can take advantage of this characteristic to influence the MTB's swimming trajectory by varying the direction of the applied magnetic field by using a simple permanent magnet (Figure 1). Taking into consideration that the magnetic force exerted on a magnetic particle is proportional to the particle's volume, due to the small size and relatively weak magnetic moment of the nanoparticles in the magnetosome chain, no significant translational force is exerted on the chain in the presence of a magnetic gradient (Bahaj
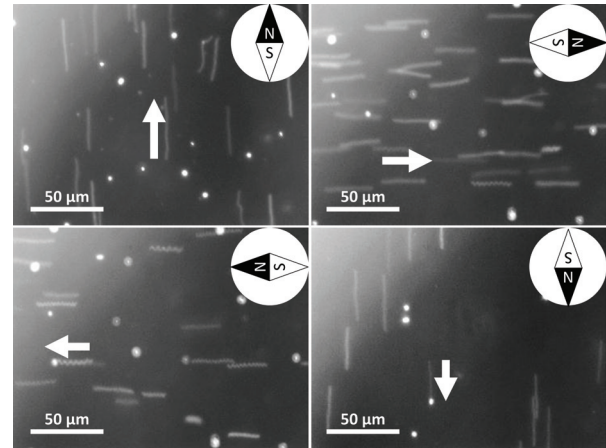
Fig. 1. Microscopic images of MTB (white lines) responding to the presence of a 2 mT magnetic field induction oriented in different directions. The white dots in the background are immobilized bacteria on the surface of the microscope slide and should be ignored. The white arrows indicate the swimming direction of the MTB. The black tip of the compass needle appearing in each frame indicates the direction of the applied magnetic field. Images were acquired using a Zeiss Imager.Z1 optical microscope in dark field reflection mode using an exposure time of 200 ms.

et al., 1996). This aspect is therefore set aside for our experiments.

The MTB used as microrobots in these experiments are of the type known as *Magnetococcus marinus* strain MC-1 (Bazylinski et al., 2013). This species of MTB has a spherical shape with an approximate diameter of 2 μm and is capable of reaching an average swimming speed of about 200 μm/s (Martel et al., 2009) by making use of its two bundles of flagella which act as propellers. These MTB can be considered as self-propelled nanomagnets that orient parallel to the surrounding magnetic field lines because of the magnetic torque exerted on their embedded chain of magnetosomes.

In order to make use of these MTB to perform microscale tasks, one must control the migration of the MTB whether individually or in a swarm (group of MTB). In this article we describe the techniques used to control MTB in order to produce 3D aggregates. Although two-dimensional (2D) aggregations can be obtained relatively easily using a single electromagnet positioned close to the sample as demonstrated in Martel and Mohammadi (2010) to build a microscale pyramid, the ability to remotely generate aggregations in a 3D volume proves to be more of a challenge.

Remotely generating 3D MTB aggregates is however better suited to our prospective future drug delivery applications since it enables us to better control and guide these microorganisms through the intricacies of the human body. The ability to do so is essential not only for medical interventions to minimize the invasiveness of interventions but
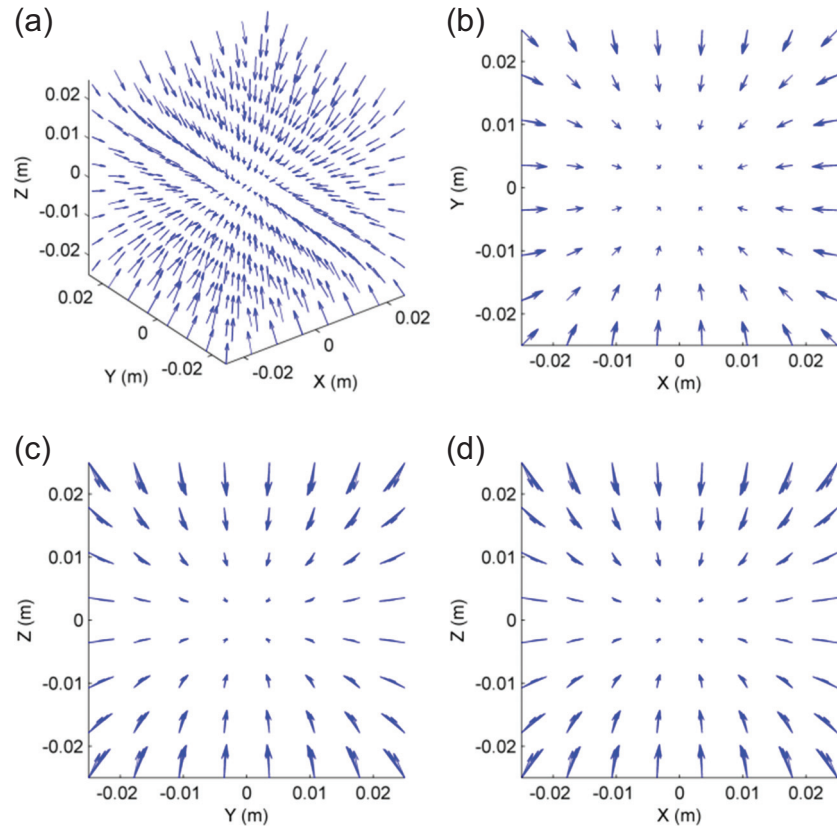
Fig. 2. 3D vector plot of a theoretical magnetic field having all its magnetic field lines oriented towards a common point in space, giving rise to a magnetic monopole: (a) 3D perspective view of the magnetic field vectors, (b) *x-y* view of the magnetic field vectors, (c) *y-z* view of the magnetic field vectors, and (d) *x-z* view of the magnetic field vectors. The arrows represent the intensity and orientation of the magnetic induction at that point.

also to better respond to different micromanipulation and microassembly tasks.

2. Model, experimental platform and simulations

Let us consider a liquid mixture containing homogenously suspended MTB. In order to aggregate the MTB contained in this solution, each one of these MTB would need to swim towards a common position in the solution (say, the center of the solution). Since the microorganisms behave magnetotactically, as shown in Figure 1, it is realistic to envision using a magnetic field to dictate the swimming trajectory of the MTB to produce such an aggregation. To do so would involve subjecting the MTB solution to a particular magnetic field geometry to orient each MTB in the solution towards a common position in the solution. Such a magnetic field geometry would require that all of its magnetic field lines be directed towards the aggregation point to force the MTB to swim towards it. Figure 2 exemplifies such a magnetic field.

This is physically impossible to accomplish using a single static magnetic field geometry since it would involve creating a magnetic monopole which would go against one of Maxwell's four equations for electromagnetism which states that the magnetic induction divergence in any point is zero

$$\nabla \cdot B = 0 \tag{1}$$

This article describes special control techniques and a platform that overcomes this limitation and aggregate MTB in a particular point in space. Mathematically, this implies producing a magnetic field geometry having a negative divergence, converging towards the desired aggregation position. This feat was accomplished in our laboratory by multiplexing different static magnetic field geometries over time creating what in essence is the addition of a fourth dimension. By proceeding in this way, we sequentially expose MTB to different magnetic field geometries for pre-defined periods of time in order to simulate the existence of a magnetic monopole.

The experimental setup designed and used for these experiments, referred to as the magnetotaxis platform, consists of three orthogonal pairs of electric coils positioned in a Maxwell configuration (Figure 3).
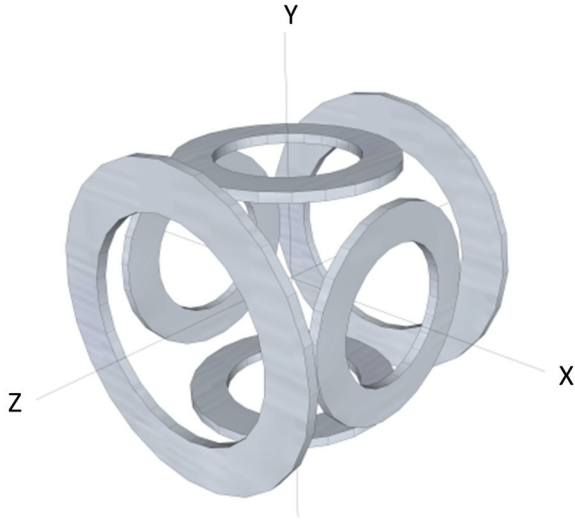
Fig. 3. Schematic representation of three orthogonal pairs of electric coils positioned in a Maxwell configuration that make-up the magnetotaxis platform used to generate different magnetic field geometries.

MATLAB (The Mathworks, Natick, Massachusetts, USA) simulations of this platform were developed to precisely map out its magnetic field. At the outset, these simulations allow us to visualize the magnetic field's intensity and orientation induced inside the platform in a 3D window (Figure 4). Then, by considering the MTB as magnetic dipoles which align perfectly with the magnetic field lines, we are able to predict the movement of the MTB subjected to the magnetic field generated by the platform.

To calculate the magnetic field generated by the platform, each electromagnet was considered as superimposed current carrying circular wires similar to the one represented in Figure 5.

Using this circular wire as a base element, the following equations derived from the Bio-Savart equation were used to calculate the radial (B_r) and axial (B_z) magnetic field components at any point (P) in space

$$B_z = \frac{\mu_0 I}{2\pi a \sqrt{(1+\alpha)^2 + \beta^2}} \left[E(k) \frac{1 - \alpha^2 - \beta^2}{(1+\alpha)^2 + \beta^2 - 4\alpha} + K(k) \right]$$
$$(2)$$

$$B_r = \frac{\mu_0 I z}{2\pi a r \sqrt{(1+\alpha)^2 + \beta^2}} \left[E(k) \frac{1 + \alpha^2 + \beta^2}{(1+\alpha)^2 + \beta^2 - 4\alpha} - K(k) \right]$$
$$(3)$$

$$\alpha = \frac{r}{a} \quad (4)$$

$$\beta = \frac{z}{a} \quad (5)$$

$$k = \sqrt{\frac{4\alpha}{(1+\alpha)^2 + \beta^2}} \quad (6)$$

where B_z is the axial magnetic field component in tesla generated by the circular wire, B_r is the radial magnetic field component in tesla generated by the circular wire, a is the radius in meters of the circular wire, r is the radial distance between the center of the circular wire and point P, z is the distance in meters along the z-axis between the center of the circular wire and point P, and $E(k)$ and $K(k)$ are respectively the complete elliptic integrals of the first and second kind.

Using these equations, therefore considering the electric coils in the platform as behaving ideally, we calculated the contribution of each electric coil in the platform, summed them up, and established the magnetic field at any point in the platform to which the MTB are exposed. Not only do these calculations allow us to visualize the magnetic field generated by the setup, but they also show the effects of multiplexing multiple magnetic field geometries over time on the swimming trajectory of MTB. Knowing that these MTB react to magnetic fields as low as 0.05 mT (Blakemore, 1975), any magnetic field having a higher value than this threshold was considered to dictate the swimming orientation of the MTB. Since the intensity of the magnetic fields to which the MTB were exposed in the experiments was higher than this threshold, the intensity of the field was ignored for simulation purposes and only the orientation of the magnetic field vector was considered to dictate the swimming direction of the bacteria.

Simulation software was developed to simulate the movement of MTB resulting from the application of sequential magnetic field geometries inside the platform. Velocity components of the MTB along each axis inside the platform were calculated using

$$v_{x,y,z} = V \frac{B_{x,y,z}}{B_{tot}} \quad (7)$$

where V represents the MTB swimming speed (200 μm/s) and B_x, B_y, and B_z represent the magnetic field components in tesla along each axis of the total magnetic field B_{tot}. A schematic representation of these values can be visualized in Figure 6.

Using this software, the position of a bacterium was periodically plotted over time following the applied time-varying magnetic field. Such a time-varying field consists of a list of magnetic field geometries (identified as configurations for our experiments), each associated with a time period during which they are applied and repeated sequentially in the platform. This list of magnetic field configurations is defined as a magnetic field sequence. Each magnetic field configuration composing the magnetic field sequence is defined as a set of currents to be applied to each coil of the platform giving rise to a unique static magnetic field geometry. These magnetic field sequences are presented as time tables, such as the one appearing in Table 1. In these time tables, a positive current value represents a current flowing in a coil in a way that its north pole is oriented
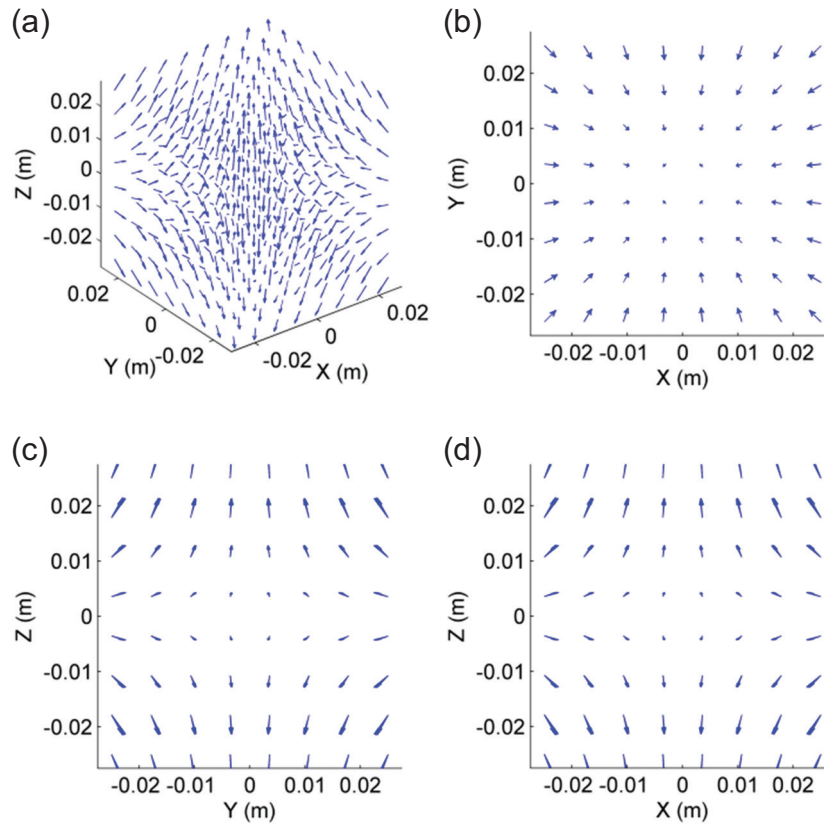
Fig. 4. Example of the resulting simulated magnetic field geometry generated inside the 3D magnetotaxis platform when both coil pairs along the *x*- and *y*-axis are each carrying 40 A oriented in a way that each electromagnet's north pole is oriented towards the center of the platform following the right-hand rule: (a) 3D perspective view of the magnetic field vectors, (b) *x-y* view of the magnetic field vectors, (c) *y-z* view of the magnetic field vectors, and (d) *x-z* view of the magnetic field vectors. The arrows represent the intensity and orientation of the magnetic induction at that point.
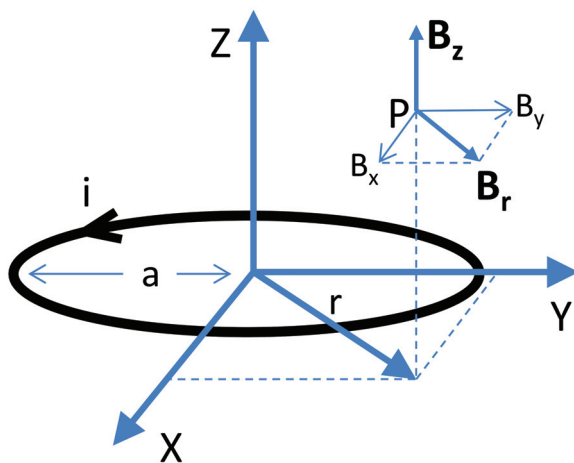
Fig. 5. Coordinate system representation of a single current carrying circular wire used as a base element for the simulation of electric coils.

Table 1. Example of a magnetic field sequence tested for convergence using our convergence algorithm.

Configuration no.	Current (A) in each coil						Exposure time(s)
	X_-	X_+	Y_-	Y_+	Z_-	Z_+	
1	40	40	40	40	40	0	3
2	40	40	40	40	0	40	3
3	40	40	40	0	40	40	3
4	40	40	0	40	40	40	3
5	40	0	40	40	40	40	3
6	0	40	40	40	40	40	3

towards the center of the platform according to the right-hand rule. Alternatively, a negative current value represents a current flowing in the opposite direction in the coil; therefore, orienting the coil's south pole towards the center of the platform.

The possibilities of magnetic field sequences that can be applied using our platform are infinite when considering that the current value of each coil, exposure time of each configuration, and the number of configurations can be varied. Even the slightest change in current value flowing
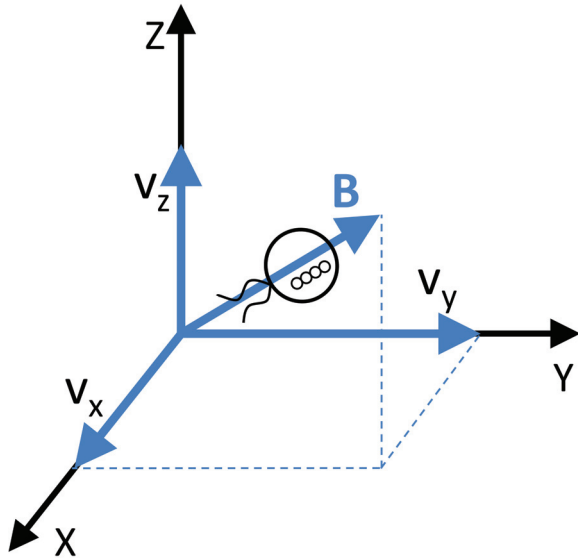
Fig. 6. Graphical representation of the magnetic field components used in the simulations to calculate the speed and direction of the MTB swimming trajectory. A schematic bacterium is presented as following the magnetic field vector *B*.

in a coil will change the geometry of the generated magnetic field for a particular configuration. For example, the magnetic field configuration appearing in Figure 4 can be generated inside the platform by activating two of the three electric coil pairs in the platform. When analyzing the generated magnetic field of this configuration, we notice that from the *x-y* point of view all magnetic field lines are oriented towards the center of the platform (Figure 4(b)) allowing an aggregation of MTB along this plane, while from the two other points of view (Figure 4(c)–(d)), we notice a divergence of the MTB along the *z*-axis. This static field therefore allows us to limit the divergence of the MTB along a single axis in the platform. By slightly modifying this magnetic field configuration and using it as a starting point, we were able to generate various magnetic field sequences cancelling out the diverging part of the static magnetic field. Doing so enabled us to generate a magnetic field sequence which when integrated over time produces magnetic field lines pointing towards the center of our platform. To identify other potentially converging magnetic field sequences, the number of activated coils in a reference configuration was iteratively changed from one to six. A standard base current of 40 A was applied for each activated coil in the configuration to ensure the presence of a minimal magnetic field of 1.5 mT at the center of the platform when a single coil is activated. Using a maximum number of six configurations within a sequence, to ensure symmetry when activating coils in our platform, we were able to identify numerous magnetic field sequences using our mathematical model. To determine if a sequence should be investigated

further, a special algorithm was designed to signal the possible existence of convergence when this magnetic field sequence was applied to the MTB sample. Since the effect of the intensity of the magnetic field on the MTB behavior is not considered for our application, magnetic field vectors for each configuration in a sequence were normalized and summed to determine the average overall swimming motion of the MTB in the controlled volume at the center of the setup. Summing up the unitary magnetic field vectors of each magnetic field configuration in a sequence, weighted with their respective application time period, allowed us to simulate the application of the different magnetic field configurations over time. The graphical representation of the simulated result of the summation of these normalized vector fields for the magnetic field sequence presented in Table 1 is illustrated in Figure 7.

The resulting vector field of Figure 7 represents the overall swimming direction of the MTB at the center of the magnetotaxis platform when exposed to the magnetic field sequence presented in Table 1. When looking at this vector field from the three different points of view (Figure 7(b)–(d)), we notice that all the vectors are oriented towards the center of the graph therefore simulating the existence of a magnetic monopole. Therefore, multiplexing different magnetic field configurations over time makes it possible to generate a virtual magnetic monopole at the center of our platform permitting us to overcome the limit presented earlier (equation (1)) which states that the divergence of magnetic induction must be zero in all points. With the use of this algorithm, different magnetic field sequences were identified as potentially having the ability to provide a reliable control of MTB in a 3D environment. These sequences are basically the fruit of trial and error experiments since there are an infinite number of possible sequences. While this algorithm indicates if a vector field converges, it does not indicate how MTB will respond in the system. A simulation of the movement of MTB in response to these magnetic field sequences was therefore required. Figure 8 illustrates such a simulation by tracking the movement of eight MTB initially positioned in each corner of a cubic volume located at the center of our magnetotaxis platform when subjected to the magnetic field sequence given in Table 1.

This simulation result theoretically validates the feasibility of aggregating MTB in a designated area by exposing different magnetic field configurations on a MTB sample using our platform. Furthermore, it also establishes that exposing MTB to time-varying magnetic fields can generate an overall average swimming migration towards the targeted point in space. This technique therefore allows us to generate aggregates of MTB in a 3D environment.

These simulations helped us identify three sequences having convergence patterns such as the one appearing in Figure 7. Magnetic sequences 1, 2, and 3 are set out in Table 2, 3, and 4.

The variable *T* in these selected sequences represents an arbitrary time exposure period during which a magnetic
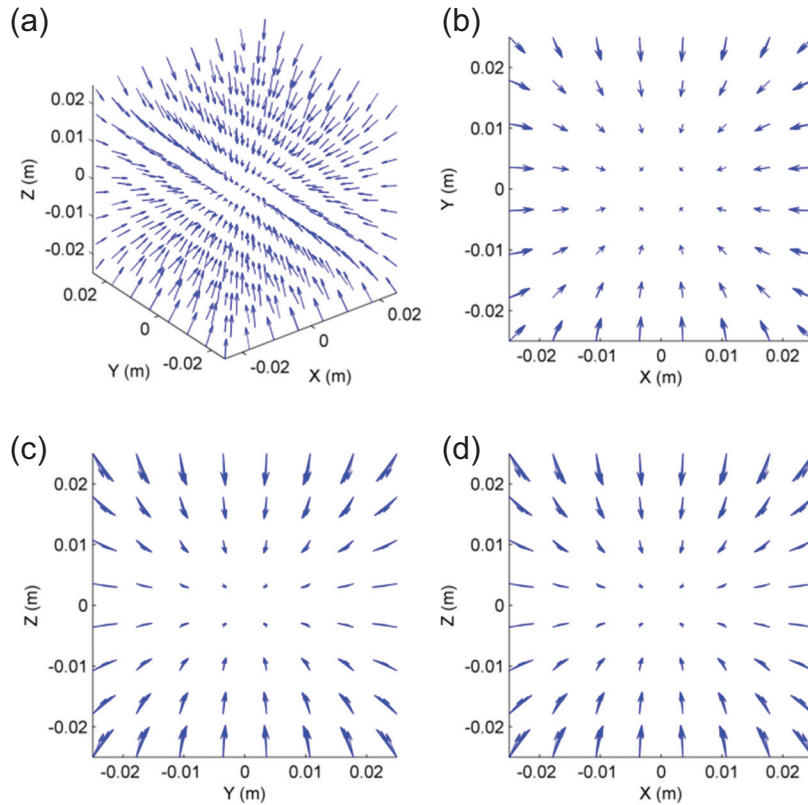
Fig. 7. 3D vector field representation of the summed normalized magnetic field configurations of the magnetic field sequence presented in Table 1: (a) 3D perspective view of the magnetic field vectors, (b) *x-y* view of the magnetic field vectors, (c) *y-z* view of the magnetic field vectors, and (d) *x-z* view of the magnetic field vectors. The vector field presented is a result obtained using our simulation software which considers each electric coil as having an ideal behavior. This vector field covers a 125 cm^3 region centered in the middle of the magnetic field setup. The arrows represent the intensity and orientation of the magnetic induction at that point.

Table 2. Magnetic field sequence 1.

Configuration no.	Current (A) in each coil						Exposure time(s)
	X_-	X_+	Y_-	Y_+	Z_-	Z_+	
1	-40	0	0	0	0	0	T
2	0	-40	0	0	0	0	T
3	0	0	-40	0	0	0	T
4	0	0	0	-40	0	0	T
5	0	0	0	0	-40	0	T
6	0	0	0	0	0	-40	T

Table 3. Magnetic field sequence 2.

Configuration no.	Current (A) in each coil						Exposure time(s)
	X_-	X_+	Y_-	Y_+	Z_-	Z_+	
1	40	40	40	40	0	0	T
2	40	40	0	0	40	40	T
3	0	0	40	40	40	40	T

field configuration is applied. This variable is used since the simulation results of these sequences demonstrated that an

aggregation of MTB was possible based on different exposure times. Having covered the theoretical aspects which
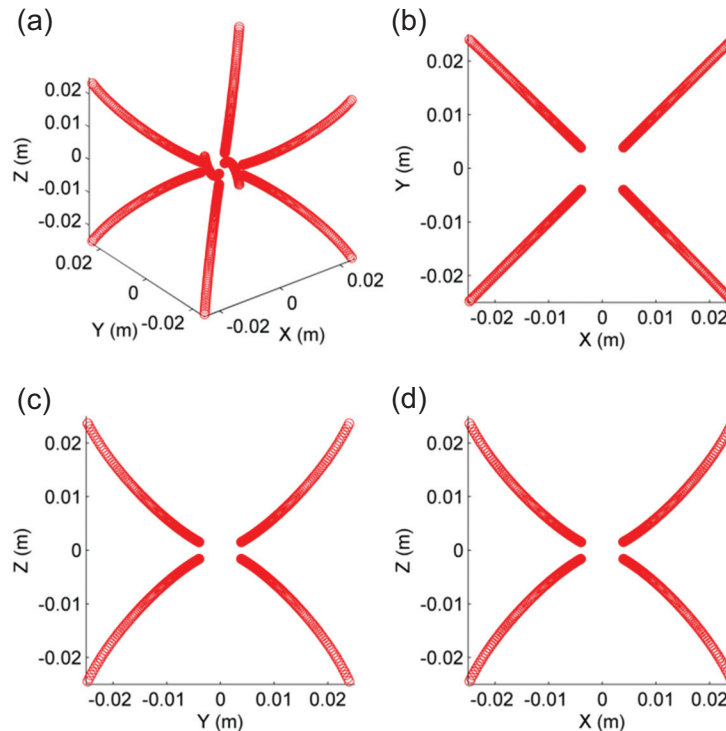
Fig. 8. Graphical representation of the simulation of eight MTB converging towards the center of a 125 cm³ volume located at the center of the experimental setup: (a) 3D perspective view of the MTB movement simulation, (b) *x-y* view of the simulation, (c) *y-z* view of the simulation, and (d) *x-z* view of the simulation. Each bacterium is initially located in one corner of the represented volume and is identified by a multitude of circles appearing as lines.

Table 4. Magnetic field sequence 3.

Configuration no.	Current (A) in each coil						Exposure time(s)
	X_-	X_+	Y_-	Y_+	Z_-	Z_+	
1	40	40	40	40	40	0	T
2	40	40	40	40	0	40	T
3	40	40	40	0	40	40	T
4	40	40	0	40	40	40	T
5	40	0	40	40	40	40	T
6	0	40	40	40	40	40	T

confirm the theoretical possibility of generating 3D aggregates of MTB using time-varying magnetic fields, we will now turn our attention to their experimental applications.

3. Materials and methods

3.1. Magnetotaxis platform

The setup used to produce the different magnetic field configurations (Figure 2) consisted of three orthogonal pairs of electromagnetic coils positioned in a Maxwell configuration. Each coil was powered by a computer-controlled XG12-140 Sorensen (AMETEK, Berwyn, Pennsylvania, USA) power source. Communication between the power supplies and the software interface was assured through universal serial bus (USB) cables simulating the existence

of a serial communication port (virtual communication port). The graphical user interface software controlling the power supplies was developed using Extensible Application Markup Language (XAML) and C# programming language. This software allows us to apply a specific magnetic field sequence composed of different magnetic field configurations by specifying the current value in each electric coil and the time period during which the current must be applied.

3.2. MTB preparation

Cells of *M. marinus* strain MC-1 were grown as previously described (Bazylinski et al., 2013) in liquid culture in 100 mL serum bottles under microaerobic conditions. MTB

were magnetically-separated at room temperature by positioning a small electromagnet directly underneath a petri dish containing a sample of the culture. By proceeding in this way, only the live MTB gathered over the tip of the electromagnet, allowing us to remove the remaining part of the culture and re-suspending the remaining MTB in phosphate buffer saline (PBS 1X) for the experiments.

3.3. Validation of MTB aggregation

The choice of the three magnetic field sequences to be tested was based on the best simulated aggregation results obtained. These sequences are the ones presented in Table 2–4. These three magnetic field sequences were first tested on MTB samples contained in a vertically oriented 5 mL clear glass vial positioned at the center of the experimental platform. An exposure time of 3 seconds ($T = 3$ s) was used for each magnetic field configuration in the sequences. Each sequence was left to run for 25 minutes after which pictures of the aggregation result were acquired from the side of the vial. Pictures of the MTB aggregation of samples placed in a petri dish were also acquired to visualize an equivalent cross-sectional area of the aggregation result in the vertical vial of each sequence. This was performed to better visualize the aggregation pattern generated by each magnetic field sequence.

In order to quantify the aggregation capacity of each magnetic field sequence tested, 1.2 μL of MTB solution was placed in a 30 mm diameter petri dish (FALCON, Mississauga, Ontario, Canada) and positioned at the center of our magnetic field setup. Each sample of MTB had an approximate initial concentration of $8 * 10^5$ MTB/mL and was subjected to one of the three magnetic field sequence for a total period of 25 minutes. Videos of the aggregation of MTB were acquired using an Aven MiniVue Digital Color Camera (Aven, Ann Arbor, Michigan, USA) equipped with a 10x magnification objective lens able to capture a surface area of approximately 375 square micrometers. The acquired videos were then processed using a MATLAB algorithm to evaluate the number MTB at each moment (in each frame) of the videos. This algorithm extracted each frame of the acquired videos and performed graphical enhancements on each image to count the number of MTB in each frame. Images were first converted to gray scale images. The contrast was then enhanced such that 1% of the data was saturated at maximum and minimum intensities. A morphological erosion and dilation using a large disk-shaped structural element was then performed to remove noise resulting from non-uniform lighting in the setup by subtracting the result of this operation from the image. The number of MTB was then counted using a disk-shaped structural element top hat filtering slightly larger than the actual size of the MC-1 MTB (2 μm) to compensate for the off focus effect when looking at a thick sample of MTB through a microscope. The signal resulting from this analysis was then considered to represent the concentration of the sample. The concentration values of MTB determined by the software for each video frame were then plotted against time. Since the number of MTB counted using this technique does not necessarily represent the exact number of MTB on the video frames, only the increase in number of MTB was plotted in the result graphs. These graphs will be presented in the section 4. This increase in concentration of MTB in the samples is defined as the concentration increase ratio. This concentration increase ratio was then calibrated using reference solutions of known MTB concentration to determine the final concentration of the samples observed in the experiments.

3.4. Validation of MTB swarm control

Taking into consideration the numerous potential applications based on the use of MTB as microrobots, the ability to generate aggregates of microorganisms using time-varying magnetic fields is insufficient. Not only must we be able to generate MTB aggregates, but we must also be able to move this aggregate in order to allow these microorganisms to act as microrobots and allow them to accomplish the envisioned microscale robotic tasks. Therefore, tests were conducted in order to validate our ability not only to generate MTB aggregates but also maintain and move the aggregation position.

Our technique to control the position of aggregation consists of using current ratio variations between the electric coils of each pair in the magnetotaxis platform. When using two electric coils positioned in a Maxwell configuration each carrying equal but opposite currents, it is possible to generate a MTB aggregation plane at the center of these two coils. By changing the current ratio between these coils, one can shift this aggregation plane based on

$$\frac{I_1}{I_2} = \sqrt{\frac{r^2 + \left(z + \frac{d}{2}\right)^2}{r^2 + \left(z - \frac{d}{2}\right)^2}}^{-3} \tag{8}$$

where r is the radius of each electromagnet in meters, z is the position in meters of the aggregation plane from the center point between the two electromagnets, and d is the distance in meters separating the two electromagnets. A demonstration of this plane aggregation between the two electric coils and the resulting shift of the aggregation position is presented in Figure 9.

This current ratio variation technique was applied to the magnetic field sequences presented in this article. By changing the current ratios between the electric coils of each pair in the setup for each magnetic field configuration in a sequence, we are able to change the theoretical MTB aggregation position. This technique was first evaluated using our simulation software. As it appears in Figure 10, an increase in the current ratio between the electric coils positioned on the *x*-axis ($I_{x-}:I_{x+}$) for sequence 3 (Table 4) induces a shift in the aggregation position in the positive direction of the axis. By switching the current ratio from 40:40 to 45:40, we can observe an approximate 1.2
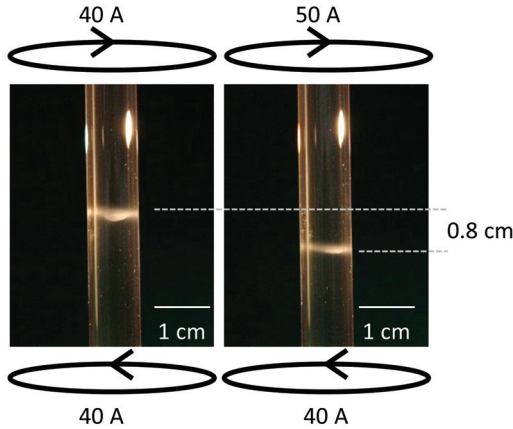
Fig. 9. Pictures of two 5 mL MTB-filled vial placed vertically at the center of the experimental platform. Planar MTB aggregations in each vial (visible as white lines) were generated by activating a single pair of electric coils. The dotted lines in the picture demonstrate our ability to shift the aggregation of MTB by varying the current ratio in the pair of electric coils.

cm shift of the MTB aggregation position in the positive direction of the *x*-axis in the simulation results presented in Figure 10. The resulting sequence used for this simulation is the sequence presented in Table 5.

Using this current ratio variation technique, we can theoretically control the movement of the MTB aggregation position within our platform and therefore in a 3D environment. In order to experimentally validate our ability to control the movement of a MTB aggregation using this technique, experiments were performed by placing 1.4 mL of suspended MTB in a petri dish positioned at the center of our experimental setup. The MTB aggregate was generated and then was moved using magnetic sequence 3 following a cross-shaped pattern based on our simulation results.

3.5. 3D aggregation

To demonstrate our ability to experimentally generate, move, and maintain a 3D MTB aggregate within a volume, a 15 mL MTB solution contained in a clear glass vial was positioned at the center of the platform. Magnetic field sequence 3 (Table 4) was applied to give rise to a MTB aggregate at the center of the vial. Once the MTB aggregate was made visible, using the previously described current ratio variation technique, we varied the current ratios in the electric coils so to make the MTB aggregate follow a rectangular trajectory within the solution. Images of the resulting MTB aggregate movement were acquired from the side of the vial.

Finally, to insure that our previous experiment was not due to chance, a 3D maze representing a chaotic network of capillaries was designed and built in order to assess our ability to remotely control a MTB aggregate within a complex environment. Since the success or failure assessment of an experiment in this study relied on what could be seen with the naked eye, this maze had to be built using a clear material. Since the MTB used in these experiments demonstrated good behavior when in contact with glass, hollow glass tubes were used to build the maze. The maze was designed using a multitude of interconnected hollow glass cylindrical tubes having an inside diameter of approximately 2 mm. This 3D glass maze was first imaged using a Siemens Magnetom 1.5T MRI after having been filled with a gadolinium-based MRI contrast agent solution (Gadoteridol, ProHance). The resulting images were then reconstructed using MATLAB to generate a 3D representation of the inside volume of the setup's capillaries to help us calibrate the magnetic field sequence used to generate and control the MTB aggregate within this maze. This reconstruction of the 3D model is presented in Figure 11.

4. Results and discussion

The results of our first experiments to remotely generate MTB aggregates using magnetic field sequences 1–3 are presented in Figure 12.

These images indicate that the resulting MTB aggregation of sequence 1 (Figure 12(a)) and sequence 3 (Figure 12(c)) generate an MTB aggregate in suspension in the medium centered in the vertical vial. Figure 12(a) and (c) therefore confirm our ability to generate MTB aggregates within a volume using magnetic field sequences 1 and 3. On the other hand, sequence 2 (Figure 12(b)) also generated MTB aggregates, but this time two distinct aggregates were generated along the sides of the cylindrical vial. This result does not allow us to state that MTB aggregation using this magnetic field sequence is possible since the sides of the vials acted as boundaries to limit the migration of the MTB. Nonetheless, since the MTB aggregates were vertically centered in the vial, we can state that a MTB aggregation still took place along the vertical axis of the experimental setup using sequence 2.

The experiment results presented in Figure 12(d)–(f) were obtained using the same conditions as in Figure 12(a)–(c), respectively, with the exception that the samples were placed in petri dishes and images were acquired from the top of the platform rather than from the side. The resulting pictures give an equivalent cross-sectional picture of the aggregations in the vertical vials. Sequences 1 and 3 both demonstrated, as anticipated, a good capacity of aggregation along the horizontal plane by creating a dense disk-shaped aggregation at the center of the petri dish (Figure 12(d) and (f)). This, along with the results shown in Figure 12(a) and (c), confirms our hypothesis of being able to generate MTB aggregates along the three axes, and therefore experimentally confirms our ability to generate 3D aggregates using time-varying magnetic fields. As for sequence 2, we notice an aggregation pattern in the
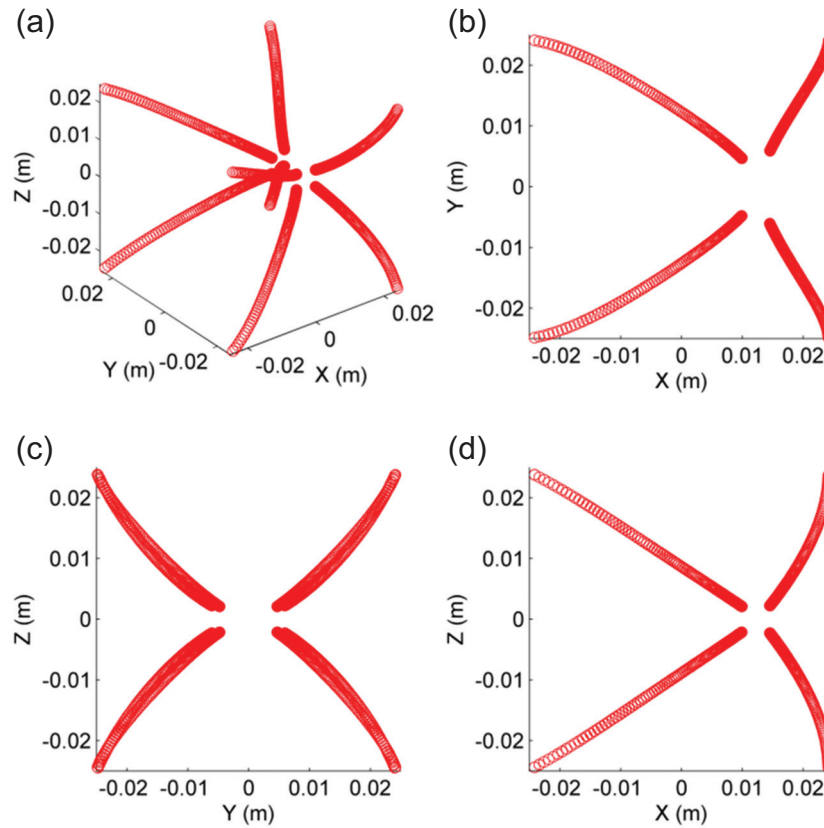
Fig. 10. Graphical representation of the simulation result of the MTB aggregation shift along the *x*-axis due to an increase from 40:40 to 45:40 in the current ratio between the electric coils on this axis of the experimental setup: (a) 3D perspective view of the MTB movement simulation, (b) *x-y* view of the simulation, (c) *y-z* view of the simulation, and (d) *x-z* view of the simulation. This simulation presents the movement of eight MTB (circles) initially located in each corner of the 125 cm^3 volume presented. The resulting sequence from this current ratio variation leading to the simulation result presented in this figure is presented in Table 5.

Table 5. Parameters of magnetic field sequence 3 with a modified current ratio for the electric coils along the *x*-axis leading to a theoretical 1.2 cm shift in the MTB aggregation position along the *x*-axis in the positive direction in the experimental setup.

Configuration no.	Current (A) in each coil						Exposure time(s)
	X_-	X_+	Y_-	Y_+	Z_-	Z_+	
1	45	40	40	40	40	0	3
2	45	40	40	40	0	40	3
3	45	40	40	0	40	40	3
4	45	40	0	40	40	40	3
5	40	0	40	40	40	40	3
6	0	40	40	40	40	40	3

shape of a cross. The lines of the cross coincide with the diagonals of the experimental platform. By referring to the simulations, we are able to understand this behavior. Simulations representing the evolution of MTB confined within a virtual petri dish were performed using the same magnetic field sequence. The result of this simulation, presented in Figure 13, shows 28 MTB initially positioned along the extremities of the petri dish periodically plotted to visualize their migration trajectory over a 25 minute period.

In this simulation result, each of these 28 MTB initially dispersed along the extremity of the petri dish deviate under the influence of the time-varying magnetic field (sequence 2) towards the closest diagonal of the experimental setup and from there migrated towards the center of the petri dish. This explains the visible pattern presented in Figure 12(e) since all of the MTB gather along the diagonals to slowly migrate towards the center of the petri dish. This is unique to this magnetic field sequence and supports the
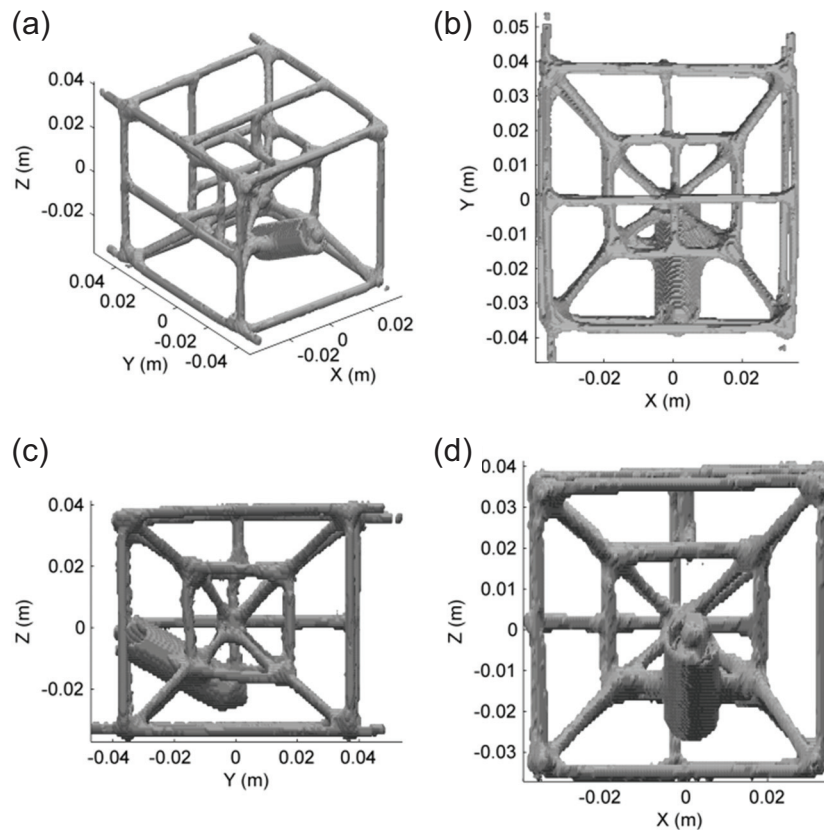
Fig. 11. 3D MATLAB reconstruction of MRI images of the 3D glass maze injected with a gadolinium-based contrast agent solution: (a) 3D perspective view of the 3D maze, (b) *x-y* view of the maze, (c) *y-z* view of the maze, and (d) *x-z* view of the maze.

aggregation shape seen in the vertical vial in Figure 12(b) since the MTB aggregation does not take place precisely at the center of the petri dish and therefore finds itself along the rounded sides of the vertical vial.

The concentration increase ratio results of the MTB aggregation videos acquired using the methods previously described are presented in Figure 14. These curves plot the evolution of the relative MTB concentration at the center of the sample positioned in the petri dish at the center of the experimental setup.

The vertical axes of the graphs in Figure 14 indicate the concentration increase ratio which refers to the number of MTB present in the field of view of the video relative to the initial number of MTB in the frame. This number represents the increase in concentration of the observed sample over time. Our first consideration when examining these curves is the end concentration of MTB that can be produced by each of these sequences at the target area. Based on our results we noticed that for a common period of 25 minutes sequences 2 and 3 were able to increase the concentration of MTB at the center of the petri dish by five to six times while sequence 1 only increased it by two to three times. This confirms that sequence 2 and 3 were more effective in terms of generating concentrated MTB

aggregates at the center of the petri dish when compared to sequence 1. This increase in MTB concentration is an important aspect when considering MTB for drug delivery applications. While this article focuses on our ability to use these MTB as microrobots by generating and steering 3D aggregates, the final MTB concentration required in drug delivery applications remains to be determined. It is possible to attach encapsulated drug to the surface of bacteria (Taherkhani et al., 2012). Preliminary experiments performed by our group show that approximately 70 liposomes, each containing drug molecules, can be attached to the surface of the MC-1 cell without significantly reducing the average velocity of each bacterium due to the increase in weight and drag caused by the therapeutic cargo. Necessary MTB concentrations will vary according to many factors such as, but not limited to, drug percentage loaded in each capsule, drug type, and tumor type. Therefore, the required MTB concentration to cause a therapeutic effect on a targeted tumor tissue remains an aspect to be analyzed.

The concentration increase ratio was also measured when varying the exposure time (T) of each sequence. MTB aggregation was measured using T-values of 1, 3, and 5 seconds. These results are plotted in Figure 14. For sequence 1, we notice a slight increase in the slope of the concentration
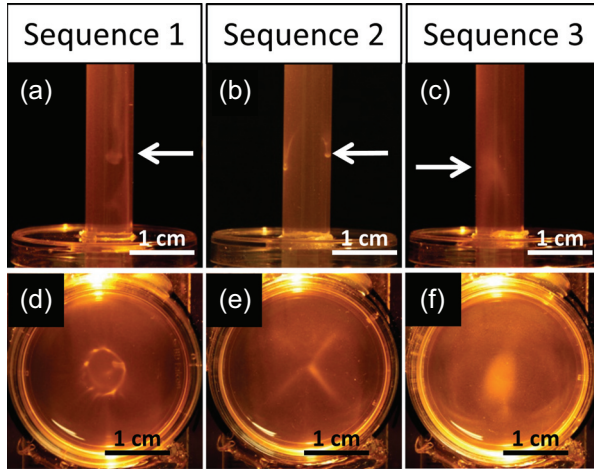
Fig. 12. Pictures of MTB aggregation results using each of the three magnetic field sequences presented in Table 2–4: (a)–(c) MTB aggregation results in a 5 mL MTB-filled vial placed vertically at the center of the experimental setup for sequences 1, 2, and 3 respectively (the white arrows point to the resulting MTB aggregation) and (d)–(f) MTB aggregation result in MTB-filled 30 mm diameter petri dish placed horizontally in the experimental setup for sequences 1, 2, and 3 respectively.
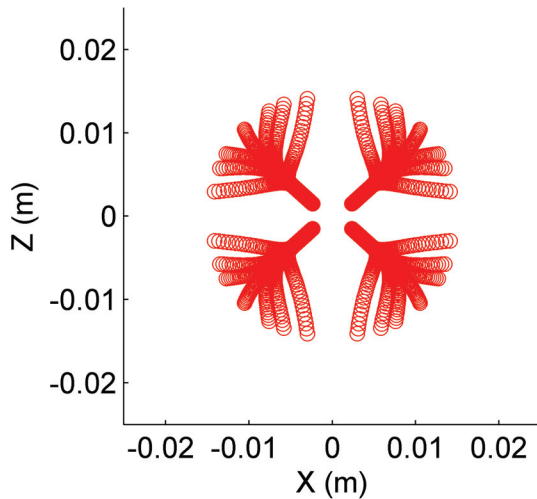
Fig. 13. Plot of the simulated migration of 28 MTB initially positioned along the extremity of a virtual 30 mm diameter petri dish positioned at the center of the experimental setup using sequence 2 with an exposure time of 3 seconds for a total period of 25 minutes.

curve having a *T*-value of 5 seconds. As for sequence 2, we notice a significant increase when subjected to a *T*-value of 1 second. In fact, the concentration increase ratio jumps from approximately 2 for exposure times of 3 and 5 seconds to approximately 5 for an exposure time of 1 second. Unfortunately, this concentration increase cannot be attributed entirely to the decrease in exposure time. The shape of the aggregate generated by the sequence must also be considered. By referring to Figure 12(e), we notice that
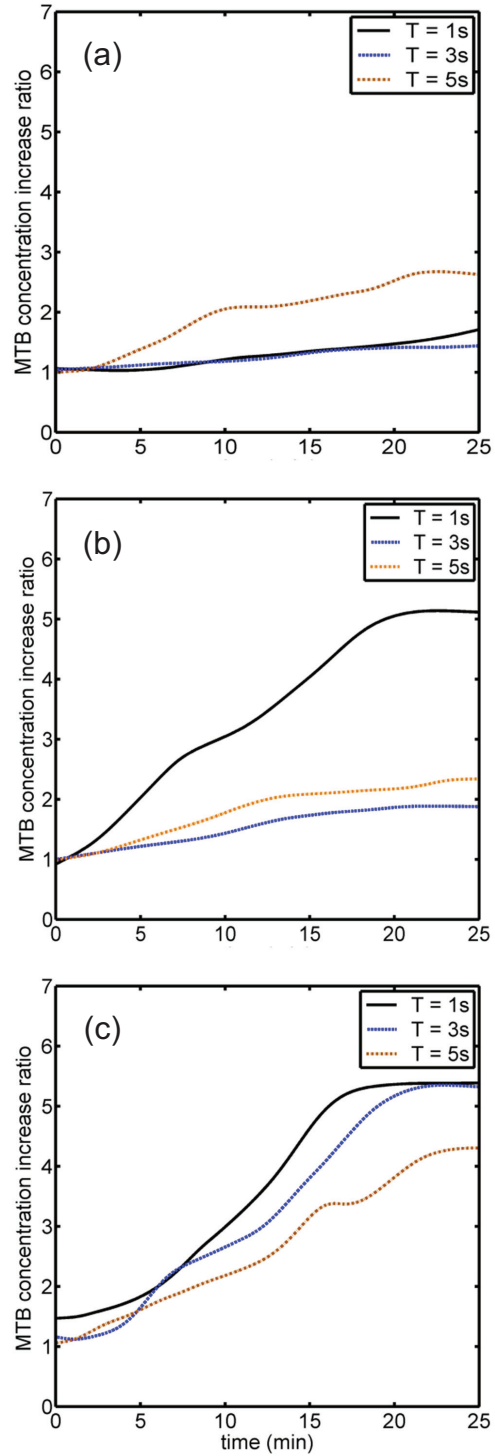
Fig. 14. Graphs of relative MTB concentration at the targeted area (middle of sample) for three different magnetic field sequences applied on a 1.2 mL MTB sample contained in a petri dish: MTB concentration increase for (a) sequence 1, (b) sequence 2, and (c) sequence 3.

the cross-shaped aggregation seems to be less concentrated at the center of the petri dish and much more concentrated

along the cross-shaped lines of the aggregate. Therefore, the increase in concentration observed in Figure 14(b) may result from the shift in the aggregation shape giving rise to an increase in concentration at the center of the petri dish. The same could also be said of the two other curves in the graphic representation. Having such an aggregation shape, it is possible that the concentrated area of MTB was not represented in the videos since the aggregation in the petri dish was not necessarily located directly at the point of observation under the microscope in the center of the petri dish.

Sequence 3 seemed to demonstrate the most reliability in terms of results and allowed us to produce an aggregate at the center of the petri dish with approximately five times the initial concentration of MTB. Furthermore, this sequence indicates a slight increase in the slope of concentration when passing from a high T-value sequence to a smaller T-value sequence. Therefore, the results of the overall effect of the variation of the exposure time indicate that a decrease in T-value increases the speed of MTB aggregation in a sample.

Figure 15 presents pictures of the experimental results demonstrating our ability to move a MTB aggregate within a petri dish following a cross-shaped pattern. Figure 15(a) and (f) show the initial and final position of the MTB aggregate located at the center of the petri dish, while Figure 15(b)–(e) show our ability to move and maintain the aggregate at the extremities of the petri dish along the horizontal axes of the platform.

The results appearing in Figure 15 confirm our ability to make use of current ratio variations within each electric coil pair in a magnetic field sequence to offset the position of the MTB aggregation within a petri dish. This is of great importance since it can now be transposed over to a 3D volume.

Using magnetic field sequence 3 (Table 4) and the current ratio variation control technique, we managed to generate and manoeuver a MTB aggregate within a clear glass vial of MTB suspension as shown in Figure 16. It is important to understand that the aggregate shown in these images was not located on the side of the vial, but was in suspension in the solution.

The current ratio variations applied in magnetic field sequence 3 were first validated using our simulation software to identify the currents to be applied in each coil to obtain the correct position of aggregation. Exposure times of each magnetic field configuration of the sequence had to be slightly modified to take into consideration the relative higher density of the MTB aggregate generated in the solution to avoid bioconvection effects (Hill and Pedley, 2005), which cause the MTB aggregate to settle at the bottom of the solution. This phenomenon was avoided by slightly increasing the exposure time of magnetic field configuration 3 of sequence 3.

Finally, using sequence 3 and the current ratio variation technique as was done in the previous experiment, we were
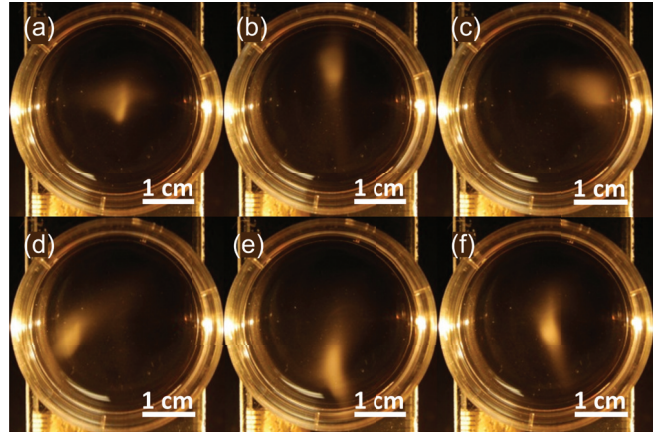
Fig. 15. Pictures of the movement of an MTB aggregate along a predetermined cross-shaped path within a petri dish positioned at the center of the platform: (a) initial position of the MTB aggregate, (b) movement of the aggregate towards the upper part of the petri dish, (c) movement of the aggregate towards the right side of the petri dish, (d) movement of the aggregate towards the left side of the petri dish, (e) movement of the aggregate towards the bottom part of the petri dish, and (f) final position of the aggregate at the center of the petri dish. The MTB aggregate was generated using magnetic field sequence 3 with an exposure time of 3 seconds. The movement of this MTB aggregate was generated using the current ratio variation technique.
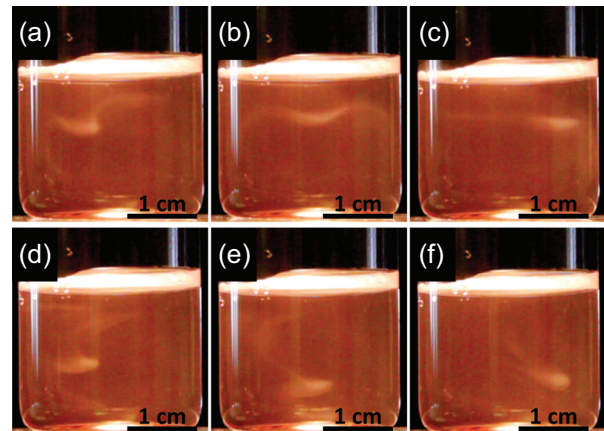
Fig. 16. Pictures showing a rectangular pattern of displacement of a MC-1 MTB aggregate (dense white blur) in a vial containing 15 mL volume of MTB solution: MTB aggregate position when focusing the magnetic field sequence on (a) the upper left part of the solution, (b) the upper middle part of the solution, (c) the upper right part of the solution, (d) the bottom left part of the solution, (e) the bottom middle part of the solution, and (f) the bottom right part of the solution.

able to successfully navigate a MTB aggregate within a chaotic network of capillaries. The results of this experiment are summarized in Figure 17. In this experiment, we successfully managed to remotely navigate a 3D MTB
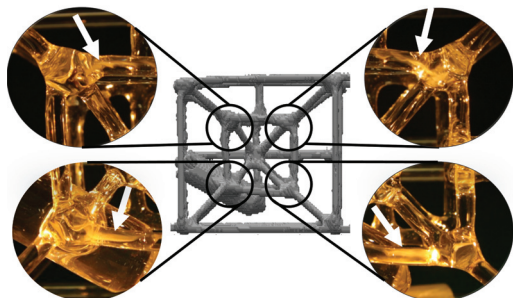
Fig. 17. 3D navigation of an MTB aggregate inside a chaotic network of interconnected hollow glass tubes. The MTB aggregate appears as a dense white spot identified by white arrows in the images.

aggregate following a square pattern outlined by the capillaries in the center of this 3D maze. Once again, using our simulation software, we identified the appropriate current offsets to be applied in each electric coil pair of the setup to direct the MTB aggregate in the proper positions to follow the square trajectory envisioned.

The result of this experiment allows us to confirm our ability to use microorganisms as a group of microrobots and navigate within complex environments, too small for most of today's artificial robots to reach. While this artificial network of capillaries cannot be compared to the network of capillaries within the human vasculature, it however allows us to state that the techniques described in this article enable us to precisely and remotely control MTB aggregates within a 3D volume.

This capacity to control MTB aggregates without the need of having a device positioned up close to the sample can lead to a variety of associated applications, such as microfabrication and lab on chip microfluidics circuits, and hopefully to the targeted drug delivery field for cancer treatment.

The results presented in this article demonstrate our ability to remotely generate and steer MTB aggregates within a 3D environment. While only three magnetic field sequences were experimentally tested, it is important to consider that optimization is possible and could be done by exploring new magnetic sequences, varying current and/or exposure time values, and even by changing the geometry of the platform.

Other important aspects such as blood flow or interstitial fluid flow will have to be considered when using these MTB for drug delivery applications. Knowing that this type of MTB can reach swimming speeds of up to 300 μm/s, controlling these MTB within the blood flow might prove to be a challenge since blood flow within normal human capillaries can reach speeds of up to 1 mm/s. However, when considering the tumor environment, blood flow tends to decrease when approaching the interstitial fluid microenvironments passed the angiogenesis network due to the interstitial fluid pressure (IFP) present in most solid tumors. It is

well known that such tumor interstitial fluid pressure (TIFP) prevents adequate diffusion of large drug molecules in the interstitial fluid environment and would allow these MTB acting as drug carriers to swim more efficiently.

5. Conclusion

In this article, we have demonstrated our ability to remotely generate and steer 2D and 3D aggregates of live MC-1 MTB within a volume of MTB cell suspension. This was achieved based on a mathematical model and the use of simulations which allowed us to predict the movement of these MTB guided by a time-varying magnetic field generated by our magnetotaxis platform. Three different time-varying magnetic field sequences were tested on MTB samples to demonstrate their aggregational capacity on MTB. Finally, the ability to move the generated MTB aggregate using our control technique was also presented and successfully tested using a complex network of capillaries resembling a 3D glass maze.

These fundamental steps are the essential building blocks to carry on our research leading to the use of MTB as microbiocarriers for targeted drug delivery applications which will hopefully soon permit local delivery of therapeutic drugs to a patient. The method presented can also be enhanced particularly in complex environments such as those encountered in targeted cancer therapies. For instance, additional techniques such as various magnetic field modulation modes taking into account the characteristics of the angiogenesis network as well as the motion behaviors of the bacteria when encountering various types of obstacles could be superimposed on such fundamental magnetic field sequences to further enhance targeting efficacy in cancer therapy. The number of different applications that can derive from this 3D MTB control is almost unlimited.

References

Abbott JJ, Nagy Z, Beyeler F et al. (2007) Robotics in the small, part I: microbotics. *Robotics and Automation Magazine*, IEEE 14(2): 92–103.

Bahaj AS, James PAB and Moeschler FD (1996) High gradient magnetic separation of motile and non-motile magnetotactic bacteria. *IEEE Transactions on Magnetics* 32(5): 5106–5108.

Bazylinski DA, Williams TJ, Lefevre CT et al. (2013) Magnetococcus marinus gen. nov., sp. nov., a marine, magnetotactic bacterium that represents a novel lineage (magnetococcaceae fam. nov., magnetococcales ord. nov.) at the base of the alphaproteobacteria. *International Journal of Systematic and Evolutionary Microbiology* 63(3): 801–808.

Benoit MR, Mayer D, Barak Y et al. (2009) Visualizing implanted tumors in mice with magnetic resonance imaging using magnetotactic bacteria. *Clinical Cancer Research* 15(16): 5170–5177.

Blakemore R (1975) Magnetotactic bacteria. *Science* 190(4212): 377–379.

Dario P, Valleggi R, Carrozza MC et al. (1992) Microactuators for microrobots: a critical survey. *Journal of Micromechanics and Microengineering* 2(3): 141.

Faivre D and Schüler D (2008). Magnetotactic bacteria and magnetosomes. *Chemical Reviews* 108(11): 4875–4898.

Felfoul O, Mokrani N, Mohammadi M et al. (2010) Effect of the chain of magnetosomes embedded in magnetotactic bacteria and their motility on magnetic resonance imaging. In: *IEEE engineering in medicine and biology society (EMBC) conference*, Buenos Aires, Argentina, 2010, pp. 4367–4370.

Frankel RB and Bazylinski DA (1994) Magnetotaxis and magnetic particles in bacteria. *Hyperfine Interactions* 90(1): 135–142.

Frankel R, Williams T and Bazylinski D (2007) Magneto-aerotaxis. In: D. Schüler (ed) *Magnetoreception and Magnetosomes in Bacteria*. Berlin: Springer, pp. 1–24.

Ghosh A and Fischer P (2009) Controlled propulsion of artificial magnetic nanostructured propellers. *Nano Letters* 9(6): 2243–2245.

Hill NA and Pedley TJ (2005) Bioconvection. *Fluid Dynamics Research* 37(1–2): 1–20.

Lins de Barros HG, Esquivel DM and Farina M (1990) Magnetotaxis. *Science Progress* 74(295): 347–359.

Martel S and Mohammadi M (2010) Using a swarm of self-propelled natural microrobots in the form of flagellated bacteria to perform complex micro-assembly tasks. In: *IEEE International conference on robotics and automation*, New York, 2010

Martel S, Mathieu JB, Felfoul O et al. (2007) Automatic navigation of an untethered device in the artery of a living animal using a conventional clinical magnetic resonance imaging system. *Applied Physics Letters* 90(11): 114105–114103.

Martel S, Mohammadi M, Felfoul O et al. (2009) Flagellated magnetotactic bacteria as controlled MRI-trackable propulsion and steering systems for medical nanorobots operating in the human microvasculature. *International Journal of Robotics Research* 28(4): 571–582.

Martel S, Tremblay CC, Ngakeng S et al. (2006) Controlled manipulation and actuation of micro-objects with magnetotactic bacteria. *Applied Physics Letters* 89: 3904.

Piotr G, Pietro T, Douglas BW et al. (2009) Propulsion of flexible polymer structures in a rotating magnetic field. *Journal of Physics: Condensed Matter* 21(20): 204110.

Sariola V, Zhou Q and Koivo H (2008) Hybrid microhandling: a unified view of robotic handling and self-assembly. *Journal of Micro-Nano Mechatronics* 4(1–2): 5–16.

Sharma NN and Mittal RK (2008) Nanorobot movement: challenges and biologically inspired solutions. *International Journal on Smart Sensing and Intelligent Systems* 1(1): 87–109.

Spring S and Bazylinski D (2006) Magnetotactic bacteria. In: Dworkin M, Falkow S, Rosenberg E et al. (eds) *The Prokaryotes*. Berlin: Springer, pp. 842–862.

Taherkhani S, Mohammadi M, Daoud J et al. (2012) Attachment of liposomes on magnetotactic bacteria acting as self-propelled drug delivery agents. In: *International conference on bioencapsulation*, Orillia, Ontario, Canada, 2012.

Tottori S, Zhang L, Qiu F et al. (2012) Magnetic helical micromachines: fabrication, controlled swimming, and cargo transport. *Advanced Materials* 24(6): 811–816.

Trimmer W and Jebens R (1989) Actuators for micro robots. In: *IEEE International conference on robotics and automation*, Scottsdale, Arizona, USA, 14–19 May 1989.

Zhang L, Abbott JJ, Dong L et al. (2009) Artificial bacterial flagella: fabrication and magnetic control. *Applied Physics Letters* 94(6): 064107-064103.